# High-resolution transmission electron microscopy imaging of misfit-dislocation networks at Cu-MgO and Cu-MnO interfaces

Groen, H.B; Kooi, B.J.; Vellinga, W.P; de Hosson, J.T.M.

*Published in:*
Philosophical Magazine A-Physics of Condensed Matter Structure Defects and Mechanical Properties

*DOI:*
10.1080/01418619908210410

PHILOSOPHICAL MAGAZINE A, 1999, VOL. 79, NO. 9, 2083–2101

# High-resolution transmission electron microscopy imaging of misfit-dislocation networks at Cu–MgO and Cu–MnO interfaces

H. B. GROEN, B. J. KOOI, W. P. VELLINGA† and J. TH. M. DE HOSSON‡

Department of Applied Physics, Materials Science Centre and Netherlands Institute for Metals Research, University of Groningen, Nijenborgh 4, 9747 AG Groningen, The Netherlands

[*Received 7 July 1998 and accepted in revised form 13 October 1998*]

ABSTRACT

Misfit dislocation networks at Cu–MgO and Cu–MnO $\{111\}_{\text{metal}}//\langle 111\rangle_{\text{oxide}}$ interfaces were studied with high-resolution transmission electron microscopy. Experimental results were compared with image simulations of tentative atomic structures of the interface region derived from lattice statics calculations. The calculations take into account the two-dimensional misfit at the interface, which is necessary given the high misfit and short repeat distances at the interfaces. The lattice statics calculations use simplified potentials across the interface which capture essential characteristics that have emerged from recent experimental results and *ab-initio* calculations. Trigonal networks of edge misfit locations with Burgers vectors $\frac{1}{6}\langle 112\rangle$ and line direction $\langle 110\rangle$ follow from these calculations. These misfit-dislocation networks have associated strain fields in the metal, stretching out from the interface with approximately the repeat distance along the interface. These strain fields show up in image simulations (along $\langle 110\rangle$ and $\langle 112\rangle$ directions) by characteristic but subtle periodic changes in contrast and brightness as well as small displacements of spots. The experimental images, also along $\langle 110\rangle$ and $\langle 112\rangle$ directions, showed similar characteristics but they were difficult to detect, especially along $\langle 112\rangle$ for the Cu–MnO interface, and may easily be missed. Judging from this evidence we conclude that the proposed misfit-dislocation structure is in fact present at these interfaces.

## § 1. INTRODUCTION

Metal–ceramic interfaces play an important role in many technologically relevant composite materials. To a large extent, the mechanical performance of these composites are controlled by the structure of the metal–ceramic interface. Precise knowledge of these interfaces would help us to understand the relation between the structure and the properties of these materials. Usually the relation between the atomic structure of the interface and its properties, for example the work of adhesion, is only determined indirectly. However, in principle the atomic structure of the interface reveals the strength of bonding at the interface directly in case of semicoherent interfaces (De Hosson *et al.* 1996, Vellinga *et al.* 1997, Vitek *et al.* 1995). The degree of

† Present address: Materials Technology, Mechanical Engineering, Eindhoven University of Technology, Den Dolech 2, Postbus 513, 5600 MB Eindhoven, The Netherlands.

‡ Email:hosson j@phys.rug.nl.

*Philosophical Magazine* A ISSN 0141–8610 print/ISSN 1460-6992 online 
http://www.tandf.co.uk/JNLS/phm.htm
http://www.taylorandfrancis.com/JNLS/phm.htm

localization of the misfit dislocations display the interaction strength across the interface; the more the Burgers vectors of edge misfit dislocations are localized along the interface, the stronger is the interaction across the interface (De Hosson *et al.* 1996, Vellinga *et al.* 1997). It is therefore of great interest to observe the interface at an atomic level. However, to quantify the relation between the structure and the strength of an interface, atomistic calculations are necessary; the experimentally observed degree of localization of misfit dislocations can be translated to bond strength with the help of the calculations.

Misfit dislocations at an interface in general constitute a two-dimensional (2D) network. Observation of these networks from edge-on high-resolution transmission electron microscopy (HRTEM) images is not straightforward owing to the projective nature of HRTEM imaging. Only in the case of a one-dimensional misfit is it possible to observe directly the dislocation cores (Kooi *et al.* 1998). It is also possible to observe the networks with weak-beam imaging, but only for systems with small mismatch and well localized dislocation cores (Mader 1992). Most metal–oxide interfaces do not meet these requirements. To discriminate between subtle differences in the interfacial structure it would be beneficial to observe the interfaces edge on along two perpendicular directions, which is not possible in most high-resolution transmission electron microscopes.

In this work the interfaces are obtained by internal oxidation of binary alloys, resulting in clean straight interfaces at an atomic scale. The orientation relations and the interface orientations are determined by the system and the oxidation parameters (Ernst 1995). Interfaces formed by parallel {111} planes of Cu–MgO and Cu–MnO, obtained by internal oxidation, were observed using a JEOL ARM 1250 electron microscope at the Max-Planck-Institut Stuttgart (Phillipp *et al.* 1994). The point resolution of this microscope is sufficient to resolve the copper matrix along a ⟨112⟩ direction, perpendicular to a ⟨110⟩ direction. This makes it possible to check an interfacial configuration that was predicted by lattice statics calculations (Vellinga and De Hosson 1996). The resulting structure of these calculations can be fed into a HRTEM image simulation program in order to compare the calculated and experimental images of the interface structure.

The Cu–MgO and to a lesser extent the Cu–MnO system have been studied before quite extensively using HRTEM (Ernst 1990, Lu and Cosandey 1992, Jang *et al.* 1993, Chen *et al.* 1994), but not in combination with atomistic calculations and not along the ⟨112⟩ direction of the metal.

## § 2. Experimental details

Interfaces between copper and MgO or MnO were created using internal oxidation of Cu–1 at.% Mg and Cu–1 at.% Mn alloys. Using this method a large number of oxide precipitates are formed in the metal matrix, allowing a large number of interfaces to be investigated. The Cu–Mg and Cu–Mn alloys were prepared by alloying the pure (99.99 wt%) components in a high-frequency furnace under an oxygen-free protective atmosphere of argon. Slices of about 1 mm thickness of the Cu–Mg ingot were oxidized in a Rhines pack (a package of copper foil containing the sample together with equal volume amounts of $Cu_2O$, copper and $Al_2O_3$ powder) in an evacuated quartz tube at 1273 K for 17 h. First, the Cu–Mn ingot was homogenized in an evacuated quartz tube for 1 week at 973 K. Subsequently, it was cold rolled from a thickness of about 4 mm to 0.5 mm. Internal oxidation of the Cu–Mn alloy was performed in a Rhines pack in an evacuated quartz tube at 1173 K for 5 h.

Specimen preparation for HRTEM work was straightforward using the standard grinding, dimpling and ion-milling tools. Ion milling was performed in a Gatan dual ion mill at 4 kV and 13° elevation. In most cases some additional ion milling (10–15 min) was done just before observation. For HRTEM the JEOL ARM 1250 in Stuttgart was used with the side-entry objective lens installed ($C_s$ = 2.7 mm; defocus spread 11 nm; semiconvergence angle 0.9 mrad (Phillipp *et al.* 1994)), resulting in a point resolution of 0.12 nm. This in principle suffices to resolve the Cu $d_{\langle 220\rangle}$ = 0.128 nm and thus allows atomic resolution images taken along Cu⟨112⟩. In one instance also a JEOL 4000 EX/II operating at 400 kV in our group in Groningen (spherical aberration coefficient, $0.97 \pm 0.02$; defocus spread, $7.8 \pm 1.4$ nm; beam semiconvergence angle, 0.8 mrad) was used. HRTEM negatives were digitized with a charge-coupled device camera and the grey scale was adapted to achieve reasonable contrast. No filtering of the images was performed.

## § 3. Results and discussion

### 3.1. *Experimental high-resolution transmission electron microscopy*

HRTEM images of edge-on observed Cu–MgO interfaces pertaining to parallel topotaxy of metal and oxide with {111} parallel to the interface are shown in figures 1 and 2 for viewing along ⟨110⟩ and ⟨112⟩ respectively. The analogous images for Cu–MnO interfaces are shown in figures 3 and 4 respectively. The image of figure 1 was recorded with a JEOL 4000 EX/II in Groningen and the images of figures 2–4 were taken using the JEOL ARM 1250.

The lattice mismatch between copper and MgO is equal to 16.5% and for Cu/MnO equal to 22.9%. Either an incoherent or one of the various possibilities of semicoherent interfaces are in agreement with the experimentally observed interface structures. The different types of misfit-dislocation network possible for parallel {111} interfaces are described in the next section. Irrespective of the type of interface structure, incoherent or semicoherent, the lattice mismatch will always determine the period of disregistry along the interface visible in HRTEM images; that is, six planes

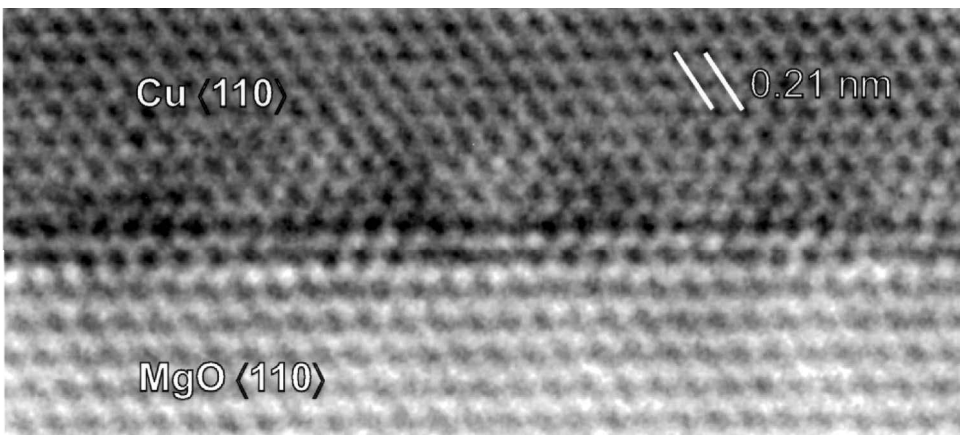


Figure 1. HRTEM image of an edge-on Cu/MgO{111} interface viewed along ⟨110⟩ in a JEOL 4000EX/II (Groningen) near optimum defocus (− 48 nm). The black dots in copper correspond to the position of the atomic columns.

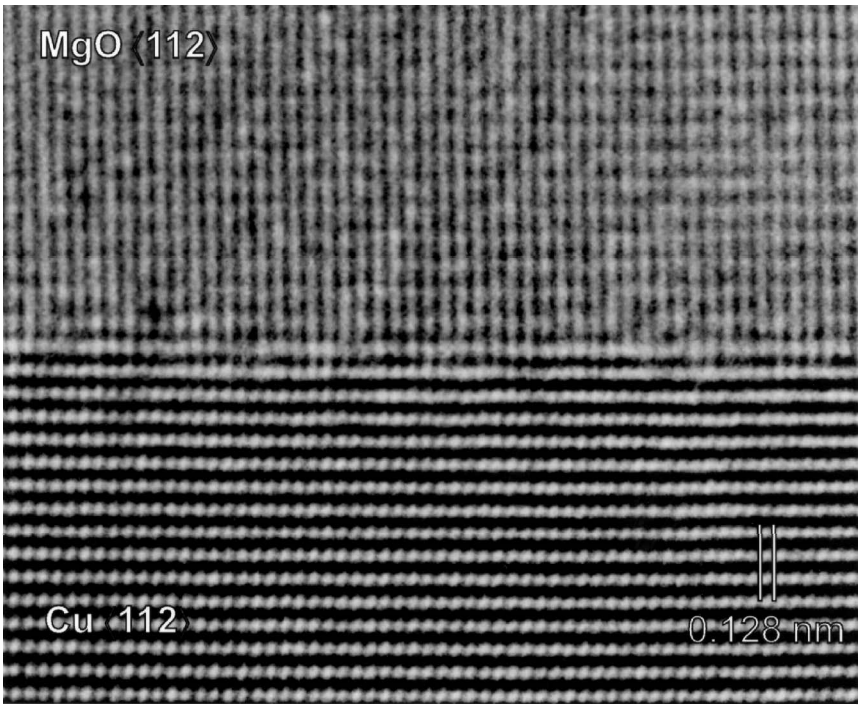


Figure 2. HRTEM image of an edge-on Cu/MgO{111} interface viewed along ⟨112⟩ in the Stuttgart JEOL ARM 1250. The defocus is about − 55 nm, and the black dots correspond to the atomic columns of copper.

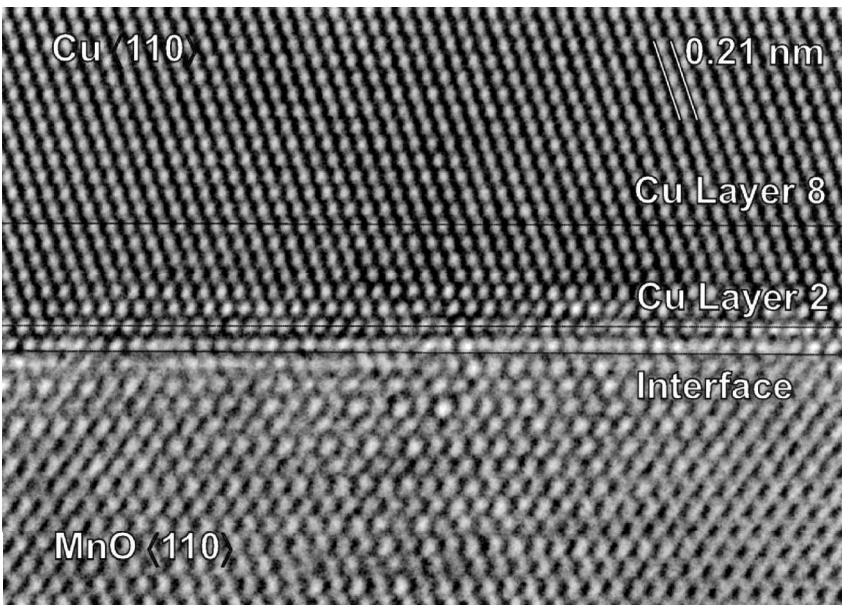


Figure 3. HRTEM image of an edge-on Cu/MnO{111} interface viewed along ⟨110⟩ in the JEOL ARM 1250. The defocus is about − 60 nm and the bright dots correspond to the atomic columns of copper.

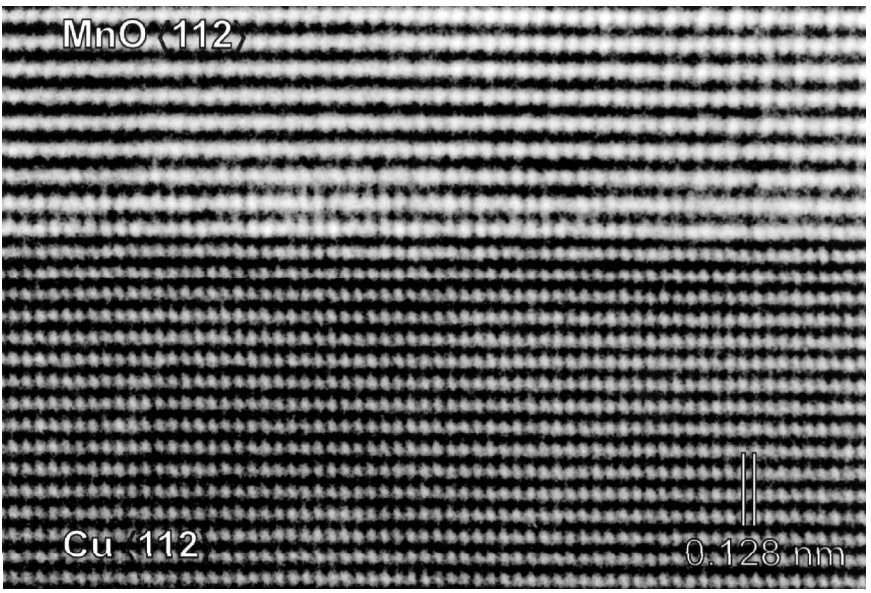


Figure 4. HRTEM image of an edge-on Cu/MnO{111} interface viewed along ⟨112⟩ in the Stuttgart JEOL ARM 1250. The defocus is about − 55 nm and the black dots correspond to the atomic columns of copper.

in MgO nearly match seven planes in copper, and four to five planes in the MnO match five to six planes in copper.

An incoherent interface can be excluded if strain fields at the interface with the predicted periodicity are visible in the experimental images. Because it is not clear *a priori* what the appearance of these strain fields in HRTEM will be, caution is necessary, since any strain field is expected to have the same periodicity as possible Moiré effects. Excluding the presence of significant Moiré effects is not so difficult for HRTEM of thin foils if firstly the interface is aligned edge on as carefully as possible with the aid of Kikuchi patterns and symmetric diffraction spot intensities and secondly the interface is atomically flat and steps or ledges do not occur in such a way that (even one plane of) the metal and oxide overlap in the viewing direction. Further, delocalization of information (point spread) (Coene and Jansen 1992) at the interface leads to a mutual overlapping of both sides of the interface in the image and therefore also yields Moiré-like effects. In particular, if field emission gun sources are used and the information for frequencies higher than the point resolution up to the information limit becomes important (for relative large defocus values), delocalization effects become significant. However, for the present high-resolution transmission electron microscopes operating at high voltages and using $LaB_6$ sources which results in a small gap between point resolution and information limit, delocalization is much less of a problem. In general, at Scherzer defocus the delocalization for linear interference is negligible for frequencies up to the point resolution of the microscope.

Still, the first metal and oxide layer at the interface can best be excluded in the analysis of strain fields. Strain fields of 2D misfit-dislocation networks consisting of displacements are complex. From the viewpoint of HRTEM imaging it is important to note that atomic 'columns' cannot be displaced on average but can be bent and

thus smear out the projected potential. The analysis of such displacement fields is not advanced in HRTEM since usually atomic columns are assumed to be perfectly straight (Möbus and Behm 1996).

Discrimination between the different types of dislocation network at semicoherent interfaces is more difficult than discrimination between an incoherent and semicoherent interface, because for all possible misfit-dislocation networks the periodicities of the strain fields are identical. Only if detailed knowledge about the strain fields is available it can be used, in principle, to distinguish the effects of the different networks in simulated and experimental HRTEM images; further discussion will follow below.

A clear sign of the presence of strain fields is difficult to detect in the HRTEM images (figures 1–4). Only in the relatively poor resolution image as taken with the JEOL 4000 (figure 1) can periodic strain fields in the copper at the interface with MgO be observed. To detect the effects of possibly existing misfit dislocation networks in the experimental HRTEM images, comparison with results of atomistic calculations, in which misfit dislocations at metal–oxide interfaces are allowed to form, appear to be essential. In the next section a description of possible misfit-dislocation networks at parallel {111} planes is given. In § 3.3 the results of atomistic calculations and their general implications for HRTEM according to image simulation are discussed. Finally, in § 3.4 a detailed comparison between individual experimental images and simulated images will be made.

### 3.2. *Misfit-dislocation networks*

Apart from an incoherent interface, different types of semicoherent interface can be proposed for the parallel topotaxy {111} interfaces (Ernst 1993) with as extremes a hexagonal misfit-dislocation network with $\frac{1}{2}\langle 110\rangle$-type Burgers vectors and $\langle 112\rangle$ dislocation-line direction and a trigonal network with $\frac{1}{6}\langle 112\rangle$-type Burgers vectors and $\langle 110\rangle$ dislocation-line direction. The hexagonal network is predicted according to the O-lattice theory by Bollmann (1970). The trigonal network can be conceived as a dissociation of the $\frac{1}{2}\langle 110\rangle$-type misfit dislocations into $\frac{1}{6}\langle 112\rangle$-type misfit dislocations for the total dislocation-line length in the hexagonal network. Since also dissociation of a part of the dislocation-line length in the hexagonal network might occur around specific dislocation nodes, an intermediate type of network between the hexagonal and trigonal is possible (Ernst 1993). The three types of network are schematically depicted in figure 5. The O nodes of the hexagonal network correspond to copper atoms in a hollow site three-fold coordinated by an oxygen atom in the terminating layer in the oxide. Nodes of the dislocation network correspond to copper atoms on top of oxygen atoms (one-fold coordination) and copper atoms in a hollow site three-fold coordinated by oxygen atoms, but corresponding to a stacking-fault position, that is with respect to first-nearest neighbours this node of the dislocation network is identical with the O nodes and only differs owing to second and more distant neighbours. Of course, dissociation in the hexagonal network starts at this last dislocation node corresponding to the three-fold-coordinated stacking-fault position and triangular intrinsic stacking-fault areas develop with the original dislocation node as centre (Ernst 1993) (cf. figure 5 (*b*)). For a finite stacking-fault energy these triangular areas will always be larger than zero (Ernst 1993). The lower the stacking-fault energy and the larger the mismatch the relatively larger the triangular stacking-fault areas become, finally completely transforming the

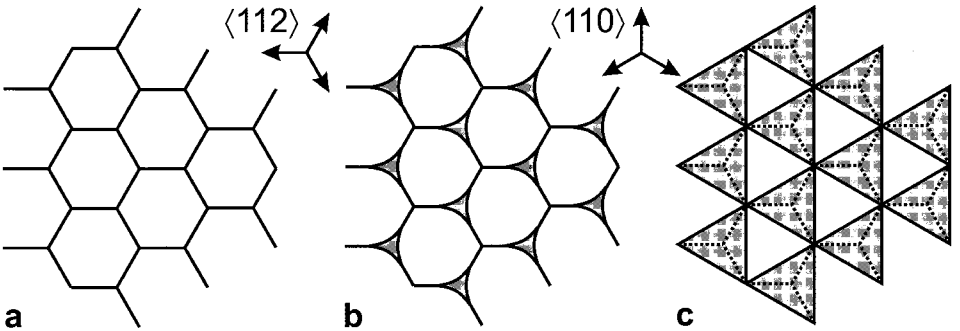


Figure 5. Schematic representation of types of misfit-dislocation network possible on interfaces formed by parallel fcc {111} (or hcp (0001)). (*a*) Hexagonal network of edge dislocations with Burgers vectors $\frac{1}{2}\langle 110\rangle$ and line direction $\langle 112\rangle$. (*b*) Hexagonal network with triangular intrinsic stacking-fault areas centred on the dislocation nodes of the original hexagonal network which have identical first-nearest-neighbour coordination as the O nodes, but different second-nearest-neighbour and more distant neighbour coordination. The edges of the triangles are bounded by $\frac{1}{6}\langle 112\rangle$ partial dislocations. (*c*) Trigonal network of edge dislocations with Burgers vectors $\frac{1}{6}\langle 112\rangle$ and line direction $\langle 110\rangle$. Increasing the relative size of the triangular stacking-fault areas in the network of (*b*), until for the total dislocation-line length the $\frac{1}{2}\langle 110\rangle$ Burgers vectors have dissociated into $\frac{1}{6}\langle 112\rangle$, results in the network of (*c*).

hexagonal network into the trigonal network. Here, the interfaces correspond to extremely high misfits and a fully trigonal network is therefore highly probable. Only a very high stacking-fault energy could possibly force the network to become hexagonal. However, the use of the concept of stacking-fault energy across a metal–oxide interface is troublesome, because of the generally large differences in lattice constants and the complex interaction mechanisms that take place across the interface. Still, some sense of the height of the stacking-fault energy can be obtained. A direct indication that the stacking-fault energy at parallel {111} metal–oxide interfaces is low comes from the observation of oxide precipitates with parallel as well as twin topotaxy within one metal matrix as for example observed for Cu/MnO (Kooi and De Hosson 1998), Pd/MgO (Lu and Cosandey 1992) and Pd/NiO (Merkle 1991, Merkle *et al.* 1992). In all these cases the precipitates are freely formed at relatively high temperatures and apart from kinetic reasons are near to equilibrium structures. Apparently, a reversal of the stacking sequence in the oxide is only of minor importance to the interfacial energy. This can be conceived as an indication that the interatomic interactions across the interface are extremely short range, that is that the second-nearest-neighbour interaction can be neglected (Merkle 1991). An important corroboration for this short range of the interactions comes from *ab-initio* calculations for parallel topotaxy {100} and {111} of interfaces Cu–MgO (Benedek *et al.* 1996). For both interfaces the region of significant non-zero charge-transfer density appeared to be only slightly greater than the interface separation (Benedek *et al.* 1996), indicating the dominance of the first-nearest-neighbour interaction. Since these arguments make clear that the stacking-fault energy at parallel {111} metal–oxide interfaces is not high, only the trigonal misfit-dislocation network at the parallel {111} interfaces of Cu–MgO and Cu–MnO is conceivable, which is also shown by Benedek *et al.* (1997) using the result of the *ab-initio* calculations in molecular dynamics and statics calculations.

### 3.3. *Atomistic calculations and image simulations*

In several studies the interfacial atomic configuration and interfacial energies of metal–oxide interfaces were determined using *ab-initio* calculations (Schoenberger *et al.* 1992, Smith *et al.* 1994, Benedek *et al.* 1996) or employing image-charge interactions (Finnis 1992, Duffy *et al.* 1993, 1996). However, in these calculations only coherent interfaces (e.g. by straining the metal to match the oxide) were considered. Lattice statics calculations appear at present more suited to determination of the relaxed atomic structure of semicoherent interfaces. The description of the interatomic interaction across the metal–oxide interface is, however, a problem, since it is poorly understood. A first important point is the range of interaction: is it short or long? Based on the image-charge scheme, long-range Coulomb interactions are involved. However, the above discussion on low stacking-fault energy for the parallel {111} metal–oxide interfaces, as deduced from *ab-initio* calculations and from oxide precipitates with parallel as well as twin topotaxy, also directly indicates that the significant interaction across the interface is short range. So, probably short-range potentials across the interface can be used, but their description remains to be developed. To overcome these problems, lattice statics calculations with very simplified interatomic interactions are used; for more details see Vellinga *et al.* (1996) and Vitek *et al.* (1995). The Finnis–Sinclair (1984) type of potentials are used to describe the interactions in the metal. The oxide is regarded as rigid and a structure unit in the oxide is replaced by a hypothetical atom (information on for example cations and anions is lost; only the geometry of the crystal and the mismatch with the metal remains). The interaction across the interface is represented by an effective pair potential as based on the Finnis–Sinclair metal potential (Ackland *et al.* 1987) multiplied by a parameter $\alpha$. By varying $\alpha$, relaxations in the metal at the interface with the oxide can be computed for different interaction strengths across the interface. This approach bears clearly severe limitations; it still generates realistic atomic-displacement fields in the metal and therefore is a useful tool for comparison with experimentally observed atomic structure information on the metal. For the Cu/MgO system a starting block, pertaining to parallel topotaxy and {111} parallel to the interface plane, was used that consisted of seven periods in the metal and six periods in the 'oxide'. This results in a mismatch of 16.67%, very close to the actual value of 16.5%. The relaxed structure for $\alpha = 2$ is shown in figure 6; figure 6(*a*) shows the results as viewed perpendicular to the interface, and figures 6(*b*) and (*c*) as viewed along $\langle 110 \rangle$ and $\langle 112 \rangle$ respectively with the interface edge on. In correspondence to the expectation of the preceding section, the resulting structure agrees with that of a trigonal network of $\frac{1}{6}\langle 112 \rangle$ misfit dislocations with alternating triangular areas of correct and incorrect stacking. The interaction parameter $\alpha$ only influences the magnitude of the relaxations and the interfacial energy, and not the type of misfit-dislocation network. For Cu/MnO the procedure is identical, apart from the misfit which is set at 25% (relative near to the actual 22.9%) by using five periods in the metal in contact with four oxide periods in the oxide. The results are therefore similar but, for a given interaction strength across the interface, the localization of the misfit dislocation cores decreases with increasing misfit (De Hosson *et al.* 1996, Vellinga *et al.* 1997).

When viewing the relaxed atomic structure in a projection along $\langle 110 \rangle$ or $\langle 112 \rangle$ with an edge-on interface (figures 6(*b*) and (*c*)), two effects can be observed: plane bending and column delocalization. Plane bending corresponds to a gradual increase in the lateral displacement of the average position of a column in a plane when

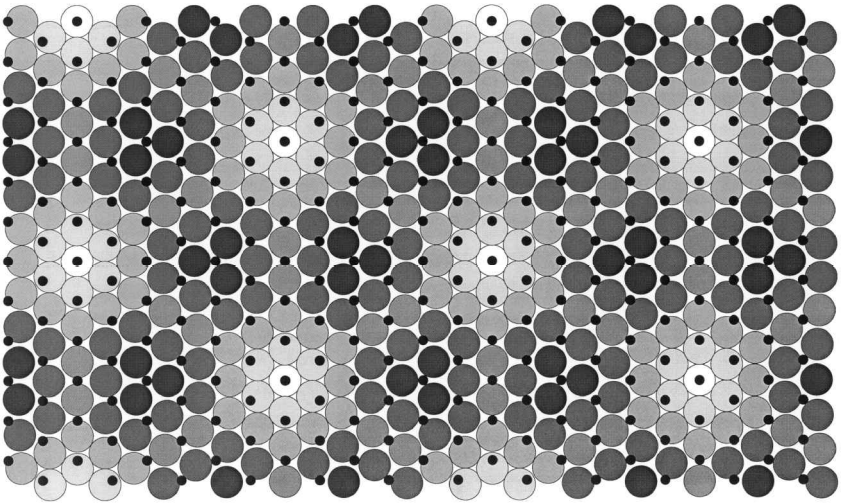

(*a*)

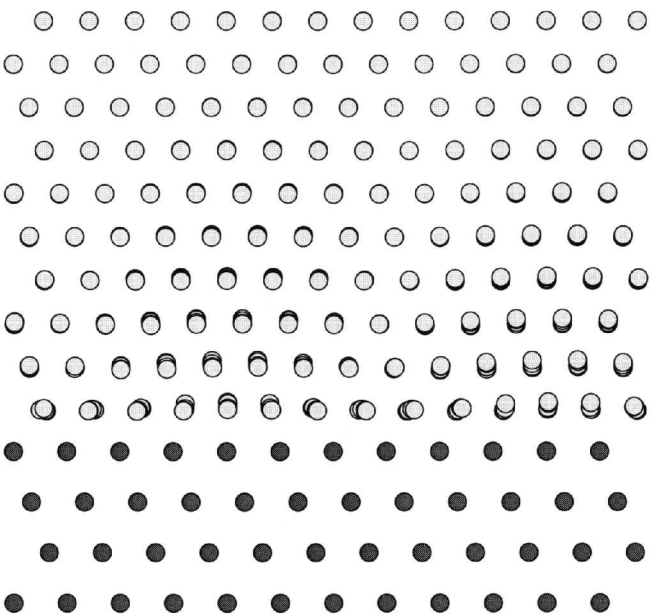

(*b*)

Figure 6. Relaxed structure (results of atomistic calculations) for the Cu/MgO{111} interface with a mismatch of 16.7% (seven periods in the metal as against six in the oxide). The factor $\alpha$ allowing simulation of different interaction strengths across the interface was given a value of two. (*a*) View along the interface normal ⟨111⟩. Small black dots denote the oxygen atoms in the terminating layer of the oxide and larger dots with different grey levels denote the copper atoms in the first layer at the interface; the darker the copper atoms, the smaller is the distance between the copper atoms and the planar interface. (*b*) View along the ⟨110⟩ with edge-on observation of the interface; black dots denote the oxygen atoms and grey dots the copper atoms. (*c*) View along the ⟨112⟩ with edge-on observation of the interface; black dots denote the oxygen atoms and grey dots the copper atoms.

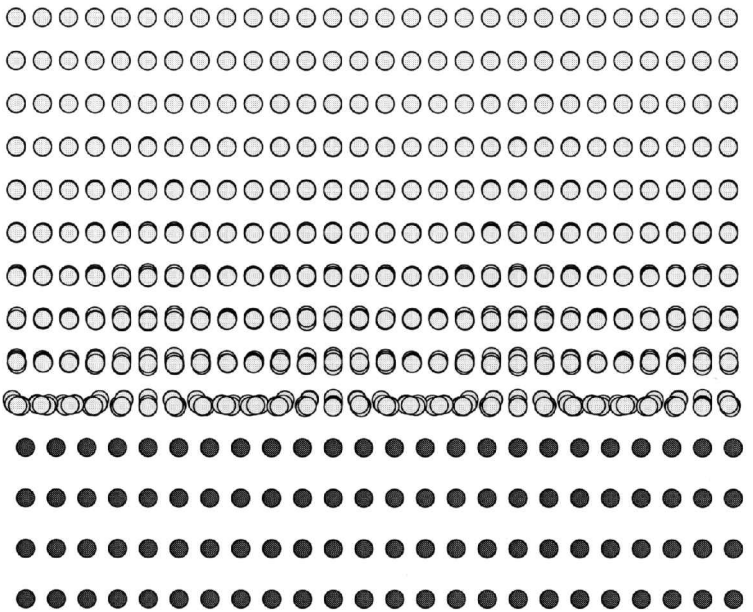

Figure 6. (*c*)

approaching the interface, and column delocalization is the result of different lateral displacements of the atoms in a column, that is corresponding to a 'spread' of the column. According to the simulated structure, plane bending is a small effect compared with column delocalization along both the ⟨110⟩ and the ⟨112⟩ directions, even for a rather strong interaction parameter $\alpha$ equal to two. Because of the trigonal structure of the network, there are always inclined dislocations present; so it is not possible to view along a core of a single dislocation (perpendicular to the Burgers vector). Therefore column bending is inevitable. The effect of this column bending on HRTEM images is not obvious. According to image simulation, column delocalization leads to brighter or darker spots in the cases when the atomic columns correspond to bright or dark spots respectively.

Viewing along the ⟨110⟩ direction (figure 6(*b*)), one of the set of $\frac{1}{6}$⟨112⟩ dislocations is viewed end on (the other two dislocation lines are inclined 60°). This is expected to correspond to a periodic variation in the distance between atomic columns along the interface and as a periodic variation in the distance of these columns to the interface, analogous to the results obtained for an end-on observed dislocation array at the Ag-$Mn_3O_4$ interface (Kooi *et al.* 1998). These effects are indeed visible in the simulated arrangement for viewing along ⟨110⟩ (figure 6(*b*)).

The relaxed block is used as input for the (multislice) MacTempas image simulation program (Kilaas 1991) after replacing the effective atoms by the true Mg–O (or Mn–O) unit and taking an oxygen layer as terminating layer of the oxide.

### 3.4. *Misfit dislocation networks; a comparison between experiment and calculations*

#### 3.4.1. *Cu/MgO* {111}//{111} *along* ⟨110⟩

Using the configuration shown in figure 6(*b*) as input for image simulation (EMS) with a thickness of 5.4 nm (size of relaxed block) and a defocus of − 48 nm

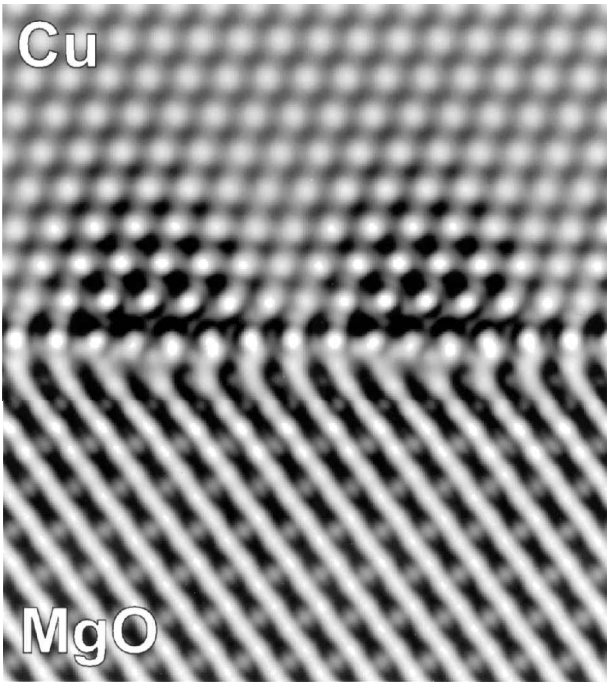


Figure 7. Image simulation (EMS) (Stadelmann 1987) on the basis of the structure shown in figure 6(*b*) for a defocus of - 48 nm (optimum defocus of JEOL 4000 EX/II) and a thickness of 5.4 nm (size of the relaxed block). The bright dots in copper correspond to the atomic columns. The larger the spreading of the atoms in a column due to bending, the darker and larger are the spots on the channels in between the columns become.

(optimum defocus of the JEOL 4000 EX/II) leads to the result shown in figure 7. The trigonal misfit dislocation network produces periodic strain-field-like effects at the copper side of the interface. In the simulation the bright dots in the copper correspond to the atomic columns and more delocalized columns give rise to relative larger dark areas around the spots than straight atomic columns of copper. Comparing this simulated image with the experimental image (figure 1), the similarity in size, shape and of course periodicity of these strain-field like effects are obvious. The further quality of the match between experiment and simulation is not optimal (depending on for example the thickness, defocus, crystal and beam tilt), but the presence of the strain-field like effect is much less dependent on these imaging parameters. For instance, if the atomic columns in copper correspond to dark spots instead of bright spots, the size, shape and periodicity of the strain fields remain similar. The extent to which the strain fields extend from the interface into the copper is related to the periodic distance between the misfit dislocations in the network. The strain fields of a coherent interface or of a single dislocation become increasingly reduced by a decreasing repeat distance between the dislocations in a network. The mismatch at the Cu–MnO interface is larger than at the Cu–MgO interface and therefore the extension of the strain fields into the copper is less for the MnO than the MgO case and this is also clearly the case for the calculated and experimental images for viewing along ⟨110⟩ (compare figures 6 and 7 of Kooi and De Hosson (1998) with the present figures 7 and 1).

3.4.2. *Cu/MgO* $\{111\}//\{111\}$ *along* $\langle 112 \rangle$

When regarding the calculated copper structure along $\langle 112 \rangle$ (figure 6(*c*)), most of the delocalization is visible in the first layer at the interface. The highest degree of delocalization in the second layer along the interface is 'out of phase' with respect to the first layer. Therefore, it is expected that the contrast or brightness variations in the first layer at the interface can be reversed with respect to the next layers. To check whether these variations at the Cu–MgO interface could be imaged in the JEM1250, image simulation was performed, the result of which is shown in figure 8 (defocus, − 55 nm; thickness, 6.2 nm; atomic columns of copper, manganese and oxygen coinciding with dark spots). To clarify the contrast variations the simulated image is averaged between the two indicated lines, including the second and third copper

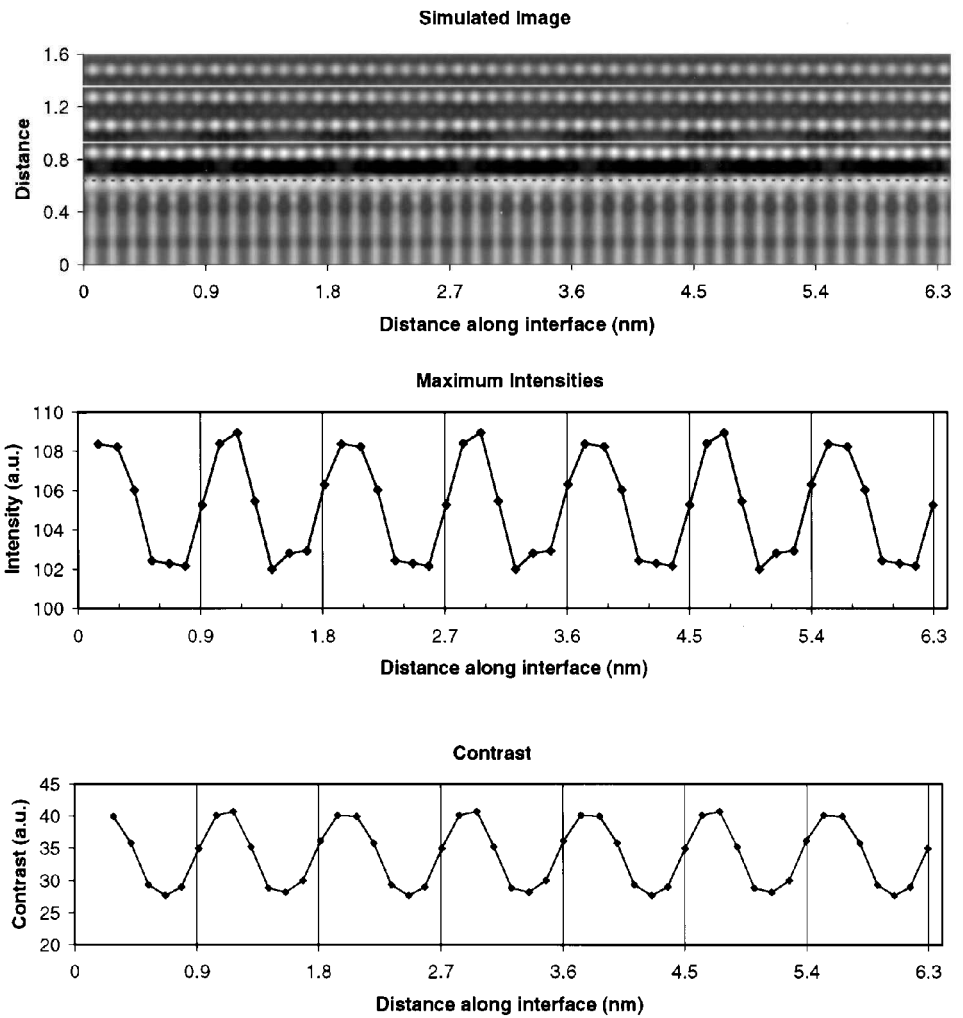


Figure 8. Brightness and contrast averaged from on top of the fourth Cu{111} layer (white lines) with respect to the interface (broken line), as a function of distance along the interface in a simulated HRTEM image (a.u., arbitrary units). The simulation is based on the structure shown in figure 6(*c*) and pertains to a defocus of − 55 nm and a thickness of 6.2 nm. The black dots in copper correspond to the atomic columns.

layers with respect to the interface. As a result the maximum brightness on the spots between the atomic columns of copper and the contrast defined as the difference in brightness between a maximum and a subsequent minima are plotted in figure 8 as functions of distance along the interface. The first layer is not regarded in the averaging because of possible influence from the oxide side of the interface (cf. § 3.1). Now the brightness and contrast variations along the interface show up clearly in the plots. Comparing the positions of the minima in the brightness and contrast plots with the disregistry observable along the interface in the image simulation, the minima along the interface are at the position of the dislocation cores. Further, as can be seen in the image simulation and as expected, the first bright layer in the copper has the brightness variations in opposite phase as the next copper layers. Needless to say, if an incoherent interface is used as basis for the image simulation instead of the semicoherent interface, the brightness and contrast variations along the interface in figure 8 vanish.

For comparison, the same procedure as used to obtain the brightness and contrast plots in figure 8 is repeated for the experimental image (figure 2) and the result is shown in figure 9. Again, the variation in brightness along the interface becomes visible. Four minima in brightness up to a distance of about 3.0 nm are present in the brightness plot of figure 9 with the correct periodicity of 0.9 nm. From 3.0 to 4.7 nm, two minima in brightness are observed whereas only one minimum at 3.8 nm is expected. Finally, in the region from 4.5 to 6.3 nm two minima are observed which are again in the correct repeat sequence with respect to the minima in the region from 0 to 3.0 nm. Less clear, the contrast seem to follow the same trend and supports the result of the brightness variations. Comparing the positions of the minima in the brightness and contrast plots with the disregistry observable along the interface in the experimental image, the minima along the interface are at the position of the dislocation cores. So, largely similar results are obtained in figures 8 and 9 and therefore the conclusion appears justified that strain fields due to misfit dislocations are present in the experimental image, although hardly detectable at first sight. This is an important issue to bear in mind before dismissing interfaces as being incoherent, because for the present high misfits the semicoherent nature of the interface is a very subtle and an easily overlooked effect in HRTEM images. The increased resolution of the JEOL ARM 1250 compared with the JEOL 4000 EX/II (0.12 nm compared with 0.17 nm point resolution) do not lead to more clearly revealed strain fields of the misfit dislocations. However, as will be shown below for the Cu/MnO(110) case, where the structure can be atomically resolved by both the JEOL ARM 1250 and the JEOL 400 EX/II, the 'excess' resolution of the JEOL ARM 1250 allows a more accurate determination of the position of the spots in the image and therefore of the displacement of spots due to (misfit) dislocations. In fact the excess resolution of the JEOL ARM 1250 appeared essential to detect the misfit dislocations on the basis of displacement of spots in HRTEM images.

An important difference between the experimental image (figure 2) and the simulated image (figure 8) is that the reversal of the brightness variations in the first copper layer with respect to the more distant copper layers is not observed. Possibly, the rigid nature of the oxide in the simulation causes this difference between the experimental results and calculations. The shear moduli of copper and MgO do not differ so much that all the mismatch would be relieved in the metal, as assumed in the atomistic calculations. In fact, elastic continuum calculations by Vellinga *et al.* (1997) showed that a substantial amount of the Burgers vector is accommodated in

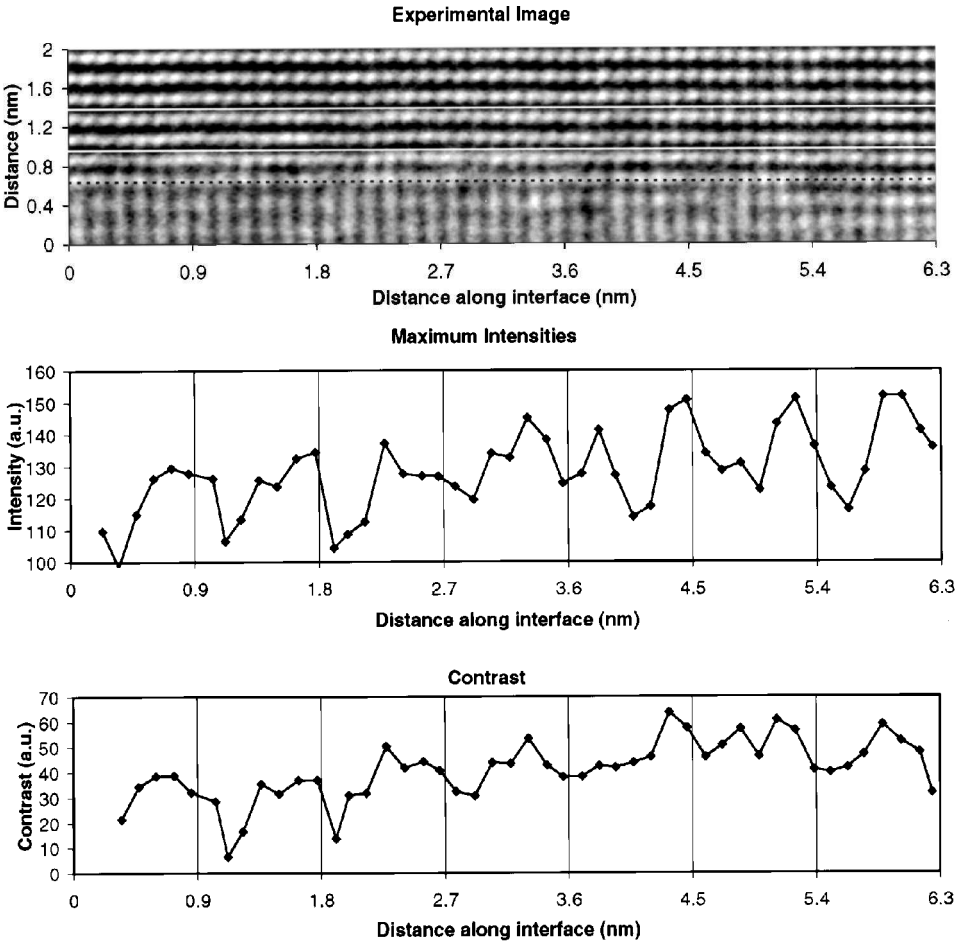


Figure 9. Brightness and contrast averaged from on top of the second to on top of the fourth Cu{111} layer (white lines) with respect to the interface (broken line), as a function of distance along the interface based on the experimental HRTEM image shown in figure 2 (a.u., arbitrary units).

the oxide, as can also be seen when looking along the ⟨110⟩ direction. Since relaxations in the oxide are not taken into account in the atomistic simulations, we expect that most of the differences between the simulated and the actual metal structures occur in the first layer at the interface. Further, the description of the interaction across the interface with pair potentials based on the Finnis–Sinclair metal potential can also be a cause for discrepancies. Discrepancies between the simulated and experimental results are then probably most evident directly at the interface, because Finnis–Sinclair potentials depend severely on the (nearest-)neighbour coordination number (Finnis and Sinclair 1984), which is rather disturbed at the interface.

### 3.4.3. *Cu/MnO* $\{111\}//\{111\}$ *along* $\langle 110\rangle$

When viewing along the ⟨110⟩ direction it is possible to measure the separation between subsequent bright dots, which correspond to (delocalized) atomic columns,

along the interface in a Cu{111} layer. First a brightness line is determined by integrating over one Cu{111} layer parallel to the interface. Secondly, the positions of each maximum is determined by fitting a third-order polynomial. (The average distance between the bright spots in the Cu{111} layer is about 20 pixels and the number of pixels around the maxima used for fitting the polynomial is 13 on average.) The resulting distance $d_{sep}$ along the interface between subsequent spots is plotted in figure 10(*a*) for the second and the eighth copper layers with respect to the interface shown in figure 3. The eighth layer is used as a reference and to check for imaging artefacts. The first copper layer is skipped because of reasons given in § 3.1. Simulations with copper and MgO blocks making an incoherent interface showed that there would only be a minor influence of the oxide on the first copper layer in the HRTEM image. The broken line in figure 10(*a*) indicates the value for $d_{sep}$ in the absence of atomic displacements, that is in strain-free copper ($d^0_{sep}$ corresponding to the $\frac{1}{4}\langle 112\rangle$ distance in copper). In figure 10(*a*) it can be seen that periodically, mostly for only one pair of subsequent spots, $d_{sep}$ is smaller than $d^0_{sep}$, whereas in between relatively larger parts along the interface correspond to $d_{sep}$ values slightly larger than $d^0_{sep}$. These observed distances clearly resemble the expected distances for an end-on observed array of misfit dislocations. The cores of the misfit dislocations are localized near the periodic smaller values for $d_{sep}$, whereas the coherent regions in between correspond to larger values than $d^0_{sep}$. Although atomic-resolution imaging of Cu/MnO$\langle 110\rangle$ is also possible in the JEOL 4000 EX/II (see figure 4 of Kooi *et al.* (1998)) it did not appear possible to obtain reasonable results approaching those shown in figure 10(*a*). The excess resolution offered by the JEOL ARM 1250 is thus very useful for accurate determination of displacement of spots in HRTEM images and as such the JEOL ARM 1250 is useful for structures which can also be resolved by microscopes with poorer resolution.

However, we do not deal with an edge-on observed array of misfit dislocations, but with a network which in the case of a trigonal network corresponds to one edge-on array and two 60° inclined arrays. To compare the experimentally based result of figure 10(*a*) with that theoretically expected for the trigonal network, the same procedure used to derive figure 10(*a*) from figure 3 is repeated, and figure 10(*b*) is derived from a simulated Cu/MnO$\langle 110\rangle$ image for a defocus of −60 nm and a thickness of 5.1 nm. Only the result of the second Cu{111} layer is shown because significant deviations from $d^0_{sep}$ do not occur in the eighth layer according to the calculations. Also, in figure 10(*b*), $d_{sep}$ is periodically smaller and larger than $d^0_{sep}$ (indicated again by the broken line). However, two important differences between the results in figure 10(*a*) and those in figure 10(*b*).

(1) The asymmetry in the lengths of the dislocation core region and of the coherent region as observed in figure 10(*a*) is absent in figure 10(*b*).
(2) The magnitude of the deviations of $d_{sep}$ from $d^0_{sep}$ is about four times larger in experiment than in theory.

Interestingly, the experimentally observed deviations of $d_{sep}$ from $d^0_{sep}$ in the second Cu{111} layer have about the same magnitude as these deviations in the first Cu{111} layer in the simulation. The results in figure 10(*b*) depend on the thickness and defocus used for the simulation, but the changes for deviations in focus and thickness which keep the bright spots on the atomic columns of copper are small and

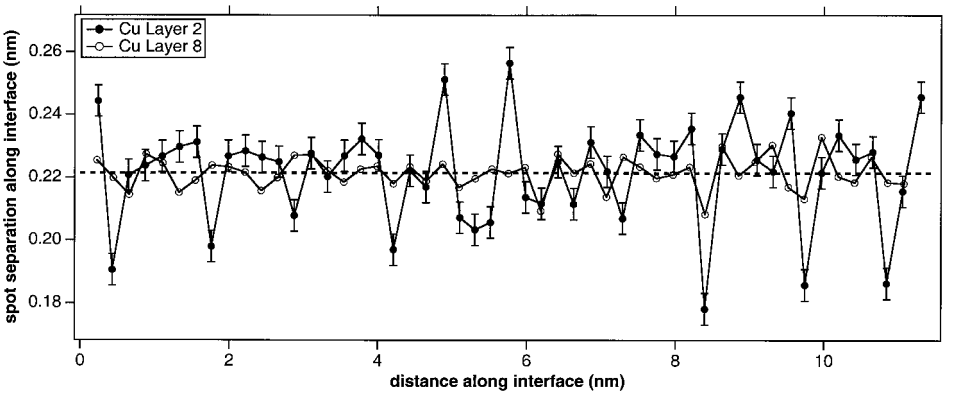


(*a*)

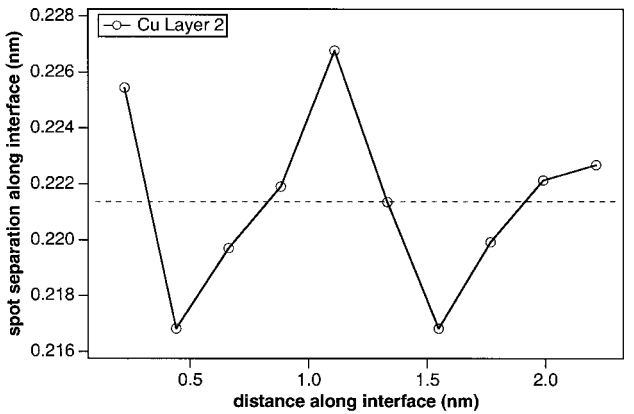


(*b*)

Figure 10. (*a*) Separation between subsequent bright spots as a function of distance along the interface for the second and eighth Cu{111} layers with respect to the interface. The results are based on the image shown in figure 3 by determining the positions of the bright spots along the interface by fitting third-order polynomials around each maximum of a brightness line profile taken on the second or eighth copper layer. (*b*) The same as (*a*) but now based on a simulated HRTEM image. The structure used for the simulation is similar to that shown in figure 6(*b*), but for Cu/MnO instead of Cu/MgO. A defocus of - 55 nm and a thickness of 5.1 nm is used.

the differences from the results in figure 10(*a*) remain more or less similar. Using beam tilt in the simulation could introduce more asymmetry in the lengths of the dislocation core region and the coherent region, but difference (2) remained. The differences probably indicate that the detailed predictions of atomic displacements by the lattice statics calculations are not correct, although the size, shape and periodicity of the strain fields are more or less predicted correctly as was shown above. The very simplified potentials, particularly the rigidity of the oxide and the use of metal pair potentials to mimic the interaction across the interface, are probably responsible for discrepancies between the simulated and experimental atomic displacements.

3.4.4. *Cu/MnO* $\{111\}//\{111\}$ *along* $\langle 112 \rangle$

Brightness and contrast variations at the Cu–MnO interface when viewed along the $\langle 112 \rangle$ direction (figure 4), analogous to the observations for the Cu–MgO $\langle 112 \rangle$ interface could not be detected. Also displacements of dark or bright spots on or in between the atomic columns of copper at the interface, indicating the presence of misfit dislocations, could not be observed. The small spacing of 0.128 nm between spots along the interface certainly does not allow determination of the periodic variations in spot separation along the interface. Periodic variations in the displacement of spots perpendicular to the interface were assumed possible, because in this direction the distance between spots is much larger, 0.209 nm. Image simulation predicted, for the bright spots in between the first and second copper layers, maximum variations of displacement perpendicular to the interface of the order of 0.003 nm. These variations are quite small despite the relatively strong interaction across the interface assumed in the simulation by taking $\alpha = 2$. Detection of these small variations in experimental images seems impossible. This was checked and indeed turned out to be the case. The 'periodic' variations in displacement of the bright spots in between the first and second copper layers in the experimental image showed variations in displacement with respect to an assumed straight interface plane with the correct magnitude. However, checking the significance of the result by repeating the same procedure for rows of spots at much larger distance (in between the tenth and eleventh copper layers) from the interface indicated that the same small variations in displacement were obtained. Hence, the small detectable deviations in displacement are determined by noise and no indication of misfit dislocations could be detected.

These observations thus indicate that, if only the Cu–MnO $\langle 112 \rangle$ interface is considered, the conclusion would be that the interface is incoherent. However, the observations along the $\langle 110 \rangle$ direction clearly indicated the presence of misfit dislocations. Furthermore, image simulation, based on a relaxed structure in which a distinct misfit-dislocation network is formed at the interface, indicates that both brightness and contrast variations and periodic variations in displacements of spots along the interface in HRTEM images for viewing along $\langle 112 \rangle$ are so small that they are probably not detectable in experimental HRTEM images. The higher mismatch of 22.9% for Cu/MnO compared with 16.5% for Cu/MgO leaves less room for any modulations due to misfit dislocations to show up in the image. It has already been shown by De Hosson *et al.* (1996) and Vellinga *et al.* (1997) that for a certain interaction strength across the interface the degree of localization of the misfit-dislocation cores decreases for increasing misfit. Therefore, for similar interaction strengths across the interface, detection of the difference between semicoherent and incoherent interfaces becomes more difficult for increasing mismatch and in this respect the misfit at the Cu–MnO interface is already extremely large. For interfaces with a relatively high misfit the incorrect conclusion can easily be drawn that the interface is incoherent, because misfit-dislocation networks at these interfaces may leave hardly a trace in experimental HRTEM images. Discriminating between a semicoherent and an incoherent interface is important for a correct understanding of the bonding of metal–oxide interfaces.

## § 4. Conclusions

The presence and character of misfit-dislocation networks at {111}//{111} Cu–MgO and Cu–MnO interfaces was studied by HRTEM. Images were recorded

for interfaces along both ⟨110⟩ and ⟨112⟩ directions and compared with image simulations. Input for the image simulations were lattice statics calculations that we believe capture the main bonding characteristics at the interface. Atomic configurations representing trigonal misfit dislocation networks were calculated, in agreement with recent experimental and theoretical evidence. These network consist of edge misfit dislocations with Burgers vector $\frac{1}{6}\langle 112\rangle$ along ⟨110⟩ directions. Image simulation showed that these networks appear in HRTEM images with the following characteristics.

(1) Periodic variations in brightness and contrast become present along the interface which can be observed as strain fields having an extension perpendicular to the interface similar to the length of the period along the interface.
(2) Periodic variations in displacement of or separation between the average position of atomic columns become present along the interface within these strain fields.

The brightness and contrast variations are caused by a variable degree of delocalization of a column, that is spreading of the atoms in a column due to bending, near the dislocation cores. Care is taken to avoid mixing these effects with Moiré effects.

Brightness and contrast variations at the Cu–MgO interface were detected for viewing along both ⟨110⟩ and ⟨112⟩ and these variations compared fairly well with those in the simulated images and thus indicated the presence of a misfit-dislocation network. Periodic variations in separation between the average position of atomic columns along the interface were detected at the Cu–MnO interface when viewing along ⟨110⟩ and also clearly indicated the presence of misfit dislocations. When viewing along ⟨112⟩, brightness variations or displacements of the average position of atomic columns are difficult to detect for Cu/MgO and could not be detected for Cu/MnO. The ability of the JEOL ARM 1250 to resolve the 0.128 nm, {220} fringes of copper is not a guarantee that the subtle effects of misfit dislocations are observed. For interfaces with high mismatch, such as Cu/MgO and Cu/MnO, the present study indicates that misfit-dislocation networks hardly leave detectable effects in HRTEM images and indicates that the incorrect conclusion can easily be drawn that the interface is incoherent.

## Acknowledgements

The authors gratefully acknowledge the Max–Planck–Institut Stuttgart for providing the opportunity to use the JEOL ARM 1250 microscope and particularly thank F. Phillipp and R. Hoschen for their assistance during the experiments.

The work described in this paper is part of the research program of the Stichting voor Fundamenteel Onderzoek der Materie Utrecht, The Netherlands.

## References

Ackland, G. J., Tichy, G., Vitek, V., and Finnis, M. W., 1987, *Phil. Mag.* A, **56**, 735.
Benedek, R., Minkoff, M., and Yang, L. H., 1996, *Phys. Rev.* B, **54**, 7697.
Benedek, R., Seidman, D. N., and Yang, L. H., 1997, *Microsc. Microanal.*, **3**, 333.
Bollmann. W., 1970, *Crystal Defects and Crystalline Interfaces* (New York: Springer).
Chen, F. R., Chiou, S. K., Chang, L., and Hong, C. S., 1994, *Ultramicroscopy,* **54**, 179.
Coene, W., and Jansen, A. J. E. M., 1992, *Scanning Microsc. Suppl.,* **6**, 379.

De Hosson, J. Th. M., Vellinga, W. P., Zhou, X. B., and Vitek, V., 1996, *Stability of Materials,* edited by A. Gonis, P. Turchi, and J. Kudrnovsky (New York: Plenum Press), pp. 581–614.
Duffy, D. M., Harding, J. H., and Stoneham, A. M., 1993, *Phil. Mag.* A, **67**, 865; 1996, *Acta mater.,* **44**, 3293.
Ernst, F., 1990, *Mater. Res. Soc. Symp. Proc.,* **183**, 49; 1993, *Phil. Mag.* A, **68**, 1251; 1995, *Mater. Sci. Eng. Rep.* R, **14**, 97.
Finnis, M. W., 1992, *Acta metall. mater.,* **40**, S25.
Finnis, M. W., and Sinclair, J. E., 1984, *Phil. Mag.* A, **50**, 45.
Jang, H., Seidman, D. N., and Merkle, K. L., 1993, *Interface Sci.,* **1**, 61.
Kilaas, R., 1991, *Proceedings of the 49th Annual Meeting of the Electron Microscopy Society of America.*
Kooi, B. J., and De Hosson, J. Th. M., 1998, *Acta mater.,* **46**, 1909.
Kooi, B. J., Groen, H. B., and De Hosson, J. Th. M., 1998, *Acta mater.,* **46**, 111.
Lu, P., and Cosandey, F., 1992, *Ultramicroscopy,* **40**, 271.
Mader, W., 1992, *Z. Metallkd.,* **83**, 478.
Merkle, K. L., 1991, *Ultramicroscopy,* **37**, 130.
Merkle, K. L., Buckett, M. I., and Gao, Y., 1992, *Acta metall. mater.,* **40**, S249.
Möbus, G., and Behm, G., 1996, *Ultramicroscopy,* **65**, 217.
Phillipp, F., Höschen, R., Osaki, M., Möbus, G., and Rühle, M., 1994, *Ultramicroscopy,* **56**, 1.
Schoenberger, U., Andersen, O. K., and Methfessel, M., 1992, *Acta metall. mater.,* **40**, S1.
Smith, J. R., Hong, T., and Srolovitz, D. J., 1994, *Phys. Rev. Lett.,* **72**, 4021.
Stadelmann, P., 1987, *Ultramicroscopy,* **21**, 131.
Vellinga, W. P., De Hosson, J. Th. M., 1996, *Mater. Sci. Forum,* **207–209**, 361.
Vellinga, W. P., De Hosson, J. Th. M., and Vitek, V., 1997, *Acta mater.,* **45**, 1525.
Vitek, V., Gutekunst, G., Mayer, J., and Ruhle, M., 1995, *Phil. Mag.* A, **71**, 1219.